'ATION PAGE

Form Approved
OMB No. 0704-0188

1

1. AGENCY USE ONLY (Leave blank)	2. REPORT DATE	3. REPORT TYPE AND DATES COVERED
	May 28, 1993	Final Report 9/30/92 to 3/31/93

4. TITLE AND SUBTITLE
Inexpensive Capillary Discharge X-Ray Laser Driver

5. FUNDING NUMBERS
N00014-92-C-2218 BASIC

6. AUTHOR(S)
Alexander M. Panin

7. PERFORMING ORGANIZATION NAME(S) AND ADDRESS(ES)
MOXTEK, Inc.
452 West 1260 North
Orem, UT 84057

8. PERFORMING ORGANIZATION REPORT NUMBER

9. SPONSORING/MONITORING AGENCY NAME(S) AND ADDRESS(ES)
Department of Defense
Strategic Defense Initiative Organization
Washington D.C. 20301-7100

10. SPONSORING/MONITORING AGENCY REPORT NUMBER

11. SUPPLEMENTARY NOTES
None

This document has been approved for public release and sale; its distribution is unlimited.

12a. DISTRIBUTION/AVAILABILITY STATEMENT
Defense Technical Information Center
Bldg. S Cameron Station
Asexandria, VA 22314-6145

12b. DISTRIBUTION CODE

13. ABSTRACT (Maximum 200 words)

In Phase I of the research we computationally modelled a capillary discharge device capable of producing the necessary plasma conditions to demonstrate ASE in argon at a wavelength of about 700 angstroms. Phase II of the research will involve the development and diagnosis of the experimental apparatus necessary to demonstrate ASE in argon. The scaling and modification of that apparatus to demonstrate ASE at shorter wavelengths using higher-Z materials will also be investigated. Future work will involve the development of robust multilayer cavity mirrors for shorter wavelengths to increase the overall intensity and usefulness of soft x-ray lasers.

14. SUBJECT TERMS		15. NUMBER OF PAGES
x-ray lasers capillary discharge	sliding spark discharge high temperature plasma x-ray sources	35
		16. PRICE CODE

17. SECURITY CLASSIFICATION OF REPORT	18. SECURITY CLASSIFICATION OF THIS PAGE	19. SECURITY CLASSIFICATION OF ABSTRACT	20. LIMITATION OF ABSTRACT
Unclassified	Unclassified	Unclassified	SAR

INEXPENSIVE CAPILLARY DISCHARGE X-RAY LASER DRIVER

FINAL TECHNICAL REPORT FOR THE PHASE I

Alexander M. Panin 5.28.93

We proposed in Phase I of the current work to compuationally model a capillary discharge x-ray laser driver which will use Ne-like argon plasma as the active medium and which will explore collisional excitation to pump upper lasing levels. During Phase I we committed to perform atomic physics calculations regarding possible lasing level pairs in Ne-like Ar, then kinetic calculations to find level populations and estimate a gain. We also expected to elaborate MHD simulation of plasma behavior in a capillary discharge and test the code by fitting it with known capillary discharge experiments.

In Phase II of the project we will build the capillary discharge x-ray laser driver according to the design of the Phase I. We will test the discharge for lasing in proposed lines.

Phase I was very successful. We have performed more than we expected in this Phase of the current Proposal.

I. ATOMIC PHYSICS CALCULATIONS.

First, making a literature survey we found that for 3-3 transitions of Ne-like Ar there are still no sufficiently reliable atomic calculations for the radiative transition probabilities. We needed values of radiative decay rates to find out which energy level pairs are candidates for lasing and eventually for a gain calculation. It was found that some high-lying level positions have also been calculated with marginal accuracy to identify transitions between them in a real plasma.

We decided to perform the required atomic physics calculation ourselves. These calculations include a determination of the energy level positions of a given multicharged ions as well as a calculation of the radiative transition rates and the branch

coefficients for the strongest and most important transitions in a multicharged ion.

We performed these calculations for Ne-like Ar, Ni-like Kr and Ni-like Mo ions. For Ne-like Ar all 36 levels with n=3 were included in the calculations, and for Ni-like ions we are able to include about 100 general levels of the n=4 configuration.

The calculations were performed by the Relativistic Perturbation Theory Method with the Model Potential of zero approximation (RPTMP). This method is well developed. It has been shown to be reliable for calculating energy levels for various isoelectronic sequences. RPTMP is especially successful in the calculation of rate constants of processes involving multicharged ions, photons, and electrons. A detailed description of method is given in the Mid-term Technical Report of current project. Here we outline the foundations of our approach which is called the energy approach [1,2].

In a nonrelativistic theory a field form procedure is connected with a diagonalization of the secular matrix. It is a standard method for a calculation of an energy shift ΔE of degenerate atomic states. Our approach is based on the Gell-Mann and Low adiabatic formula and on a perturbation expansion of a scattering matrix. We use an analogous scheme with an electroth electrodynamics scattering matrix. The perturbation expansion for the energy has only even powers. The contributions are usually presented in the form of Feynman diagrams. An important advantage of the approach is the effective inclusion of high-order perturbation theory (PT) corrections.

The method was tested to compare calculations with experimental measurements for transitions in Ne-like ions and was found to have accuracy better than 1000 cm^{-1} for level positions for elements with $Z < 50$.

A more detailed description of the calculation scheme as well as the results of our calculations in the form of tables for three mentioned ions was presented in the mid-term report on current proposal.

Here we discuss only the transitions in Ne-like Ar, and Ni-like ions of Kr and Mo we found to be most promising for lasing in a capillary discharge.

Ne-like Ar.

In Ne-like Ar these transitions are:

$$2p_{1/2}\ 3p_{3/2}\ [J=2] - 2p_{1/2}\ 3s_{1/2}\ [J=1],\quad \lambda = 69.76 \quad nm,$$

$2p_{3/2}\ 3p_{3/2}$ [J=0] - $2p_{3/2}\ 3s_{1/2}$ [J=1], λ =43.07 nm,
$2p_{1/2}\ 3p_{1/2}$ [J=0] - $2p_{1/2}\ 3s_{1/2}$ [J=1], λ =71.25 nm,
$2p_{1/2}\ 3p_{1/2}$ [J=1] - $2p_{1/2}\ 3s_{1/2}$ [J=1], λ =72.75 nm.

Special attention should also be paid to the level $2s2p^6 3s$ [J=0] which corresponds to the excitation of the 2s electron. The energy of this level excitation in Ne-like Ar is comparatively high (330 eV); nevertheless, the electron collision rate for its population is high enough to provide an efficient inversion population relative to the low active level $2p_{3/2}3s_{1/2}$[J=1]. So the search for lasing at the transition

$2s_{1/2}\ 3s_{1/2}$ [J=0] - $2p_{3/2}\ 3s_{1/2}$ [J=1], λ =15.73 nm,

in Ne-like Ar will be of significant interest.

Ni-like ions.

A Ni-like ion is much more complex to compute than Ne-like one. Nevertheless, the RPTMP method was also successfully applied to such a complex ion.

Ni-like Kr.

The numerical results of calculation for states $3p^6\ 3d^9$ 4s, 4p, 4d, 4f and $3p^5\ 3d^{10}$ 4s, 4p, 4d, 4f of Ni-like krypton are given in Table 2 of the mid-term technical report for Phase I of the current Project. In this table we calculated position, lifetime, and a probability of radiative decay to the ground state for each of the 92 levels of Ni-like Kr. The strongest radiative transition channel as well as the wavelength of this transition and a branch factor were also calculated for each of these 92 levels.

For Ni-like ion, levels $3d_{3/2}\ 4p_{1/2}$ [J=1], $3d_{3/2}\ 4p_{3/2}$ [J=1], and $3d_{3/2}\ 4p_{3/2}$ [J=1] can serve as low active levels.

Four laser transitions were found as most possible in Ni-like Kr:

$3d_{5/2}\ 4d_{5/2}$ [J=0] - $3d_{3/2}\ 4p_{1/2}$ [J=1], λ =31.21 nm,
$3d_{3/2}\ 4d_{3/2}$ [J=0] - $3d_{3/2}\ 4p_{1/2}$ [J=1], λ =42.56 nm,
$3d_{3/2}\ 4d_{3/2}$ [J=1] - $3d_{3/2}\ 4p_{1/2}$ [J=1], λ =41.50 nm,
$3d_{3/2}\ 4d_{5/2}$ [J=2] - $3d_{3/2}\ 4p_{3/2}$ [J=1], λ =41.78 nm.

The above outlined approach gives us a quick method for evaluating laser possibilities for any ion. Nevertheless, it is necessary to look completely through the transition probability matrix to determine the second and third most important decay channels. Thus

we are able to understand that in Kr IX the decay from the high active levels is almost equally distributed between three low active levels. The most favorable cases are for $3d_{3/2}\ 4d_{3/2}$ [J=0] and for $3d_{5/2}\ 4d_{5/2}$ [J=0] high active states. They have a relatively large branch coefficient for the transitions to low active level. A high active level $3p_{3/2}\ 4p_{3/2}$ [J=0] is also shown which corresponds to fast 3p subshell excitation.

It was found that at the same electron temperature, the collision excitation rate of this level is approximately the same as the excitation rate of both of the above-mentioned levels with J=0. However, there is no well-separated dominant channel for a radiative transition into the fast releasing low active level. Nevertheless, this level may influence populations of upper laser levels in the plasma.

Ni-like Mo ion.

Calculations similar to those for Kr were performed for Ni-like Mo. The Mo plasma could serve as an active medium in evacuated capillary discharge with Mo electrodes or a capillary filled with a gaseous Mo compound.

The following transitions were found to be promising for lasing in Ni-like Mo.

$3d_{5/2}\ 4d_{5/2}$ [J=0] - $3d_{3/2}\ 4p_{1/2}$ [J=1], λ =17.98 nm,
$3d_{3/2}\ 4d_{5/2}$ [J=2] - $3d_{3/2}\ 4p_{3/2}$ [J=1], λ =25.15 nm,
$3d_{3/2}\ 4d_{3/2}$ [J=1] - $3d_{3/2}\ 4p_{1/2}$ [J=1], λ =25.37 nm.

The first two should have approximately the same order of intensities, and the last one is less intense. In Ni-like Mo two very high positioned levels $3p_{3/2}\ 4p_{3/2}$ [J=0] and $3p_{1/2}\ 4p_{1/2}$ [J=0] are also strongly excited by electron collisions and are promising to serve as upper laser levels. According to our calculations they are well populated by electron collisions and have rather high branch factors for transitions to lower active levels. Thus, the short-wavelength lines

$3p_{1/2}\ 4p_{1/2}$ [J=0] - $3d_{3/2}\ 4p_{1/2}$ [J=1], λ =6.80 nm,
$3p_{3/2}\ 4p_{3/2}$ [J=0] - $3d_{3/2}\ 4p_{1/2}$ [J=1], λ =7.35 nm,

could be of interest for lasing and should be experimentally investigated in more detail by spectroscopic methods.

The level $3d_{3/2}\ 4d_{3/2}$ [J=1] is not included in this scheme because it was found to have too small branch coefficients for transitions to the low active levels.

II. PLASMA KINETICS CALCULATIONS.

Calculation of the kinetics of level excitation and deexcitation was performed to find level populations and a gain in proposed lines. For Ne-like ions this resulted in the creation of a computer code named "POPULAT.ICN". The code calculates (for a given electron density and temperature) the populations of levels involved into consideration versus time. General rate equations in the following form were used to calculate the population of specific level n:

$$\frac{dN_n}{dt} = \sum_k [N_k(N_e C_{kn} + A_{kn} G(\tau) - N_n N_e C_{nk}] +$$
$$+ N_e [N^{i-1} I_{on}^{i-1} - N_i I_n^i + N^{i+1}(R_{rr} + R_{cr} + R_{de})]_{on}$$

Here N_e = electron density, cm^{-3}; N_k and N_n = density of population of levels n and k, cm^{-3}; A_{kn} = radiative decay rates, sec^{-1}; C_{kn}, C_{nk} = electron collisional deexcitation rates from an arbitrary level k to lower specific level n and vice versa, $cm^3 sec^{-1}$. The escape factor $G(\tau)$ (where τ is optical depth of plasma) is introduced here to account for the effect of reabsorption [3,4]. I and R are ionization and recombination rate coefficients for excitation from adjacent species (Na-like and F-like ions, respectively), $cm^3 sec^{-1}$. The subscripts rr, cr, de and stand for radiative, collisional and dielectronic recombination rates.

At present we have completed the calculation of level populations for Ne-like argon. 37 levels of Ne-like Ar are included in the calculations, including the ground state, all 26 excited states of the $2p^5 3l$ (l=s,p,d) configuration, and all 10 states of $2s2p^6 3l$ (l=s,p,d) configuration. Collisional excitation and deexcitation rates for Ne-like Ar were also calculated using the above described RPTMP method. This was very time consuming but an important part of the current work. The rates of excitation and deexcitation (in a plasma with parameters of interest for lasing in proposed lines) turned out to be much higher than those between different ion species. Taking into account a long lifetime for a capillary discharge plasma (compared with the ionization balance change time), we facilitated the first run of kinetics calculations by omitting the influence of neighboring species on a population. Nevertheless, the inner-shell ionization of Na-like ions (the

process creating excited states of Ne-like Ar) was found to compete with collisional excitation from the Ne-like ground state and will be included in a more detailed kinetics calculation scheme, which we plan to run in the Phase II.

The present code calculates temporal progress of population, with logarithmic time increments. We assumed for initial conditions (at t=0) that a population of the ground state of Ne-like Ar is unity (100%) and all other states are empty (N_k=0, k≠0). This assumption may not be valid in a real plasma but it does not influence the final result, which is the same for different initial population distributions.

In Table 1 we represent the calculated level populations for Ne-like Ar in a plasma for electron densities $N_e = 10^{18}cm^{-3}$ and $10^{19}cm^{-3}$, and temperatures T_e = 30 eV and 60 eV. At these temperatures an abundance of Ne-like ion in a steady-state plasma with an established ionization equilibrium was found to be 10% and 80% respectively. According to our calculations, the time required to establish populations within Ne-like ions for these plasma parameters is much less than the time for establishment of an ionisation equilibrium. Generally this time is found to be less than several nsec. After this time a permanent inversion population between several 3p and 3s levels is established. As an example, the temporal history of populations is shown in Fig. 10, 11 for a temperature of 60 eV and densities of 10^{18} cm^{-3}, and 10^{19} cm^{-3}. Numeration of levels in Table 1 and in Figs 1,2 correspond to those in Table 1 of the Phase I Mid-term Report. Levels 2 and 4 represent lower laser 2p3s active levels. Levels 10, 11, 12, 14 and 28 represent upper 2p3p levels. As was expected, in a plasma with higher electron density the populations are established faster.

As an example, time history of population of these 7 levels is presented in Fig. 1 and 2 for two different electron densities in a capillary discharge plasma.

Final populations for different electron densities and temperatures are shown in Table 1. In this table we keep the same level designations as in Table 1 of the mid-term report.

Table 1. Populations N_n of levels in quasi-steady-state Ne-like Ar plasma. Populations presented as a fraction of total population of Ne-like Ar in plasma for different electron densities N_e(in $10^{18}cm^{-3}$) and temperatures T_e (in eV). Level 0 represents a ground state, levels 2 and 4 represent lower possible active levels, and levels 10, 11, 15 and 28 represent upper possible laser active levels.

	T_e (eV)		30	60	30	60
	N_e (10^{18} cm^{-3})		1	1	10	10
#	Level	J				
0	$2s^22p^6$	0	.9965	.6874	.9969	.7437
2	$2p_{3/2}3s_{1/2}$	1	.17 E-05	.13 E-03	.97 E-05	.67 E-03
4	$2p_{1/2}3s_{1/2}$	1	.57 E-06	.40 E-04	.35 E-05	.23 E-03
10	$2p_{1/2}3p_{1/2}$	1	.44 E-05	.30 E-03	.36 E-04	.23 E-02
11	$2p_{1/2}3p_{1/2}$	0	.31 E-05	.13 E-03	.25 E-04	.13 E-02
12	$2p_{1/2}3p_{3/2}$	2	.82 E-05	.56 E-03	.56 E-04	.37 E-02
15	$2p_{3/2}3p_{3/2}$	0	.29 E-04	.24 E-02	.71 E-04	.54 E-02
28	$2s_{1/2}3s_{1/2}$	0	.53 E-06	.59 E-04	.41 E-05	.53 E-03

According to the kinetics calculations, the most favorable conditions for inversion population between upper levels 10, 11, 12 and lower level 4 occur at electron temperatures $T_e \simeq$ 40-50 eV and densities around $10^{19}cm^{-3}$. For the shorter wavelength transition 28-2 the temperature should be slightly higher (60+ eV) and the inversion is generally less.

This code is currently being modified to account for an excitation from neighboring species, mainly from Na-like ion for our temperature range (both from ground and excited states). It seems to be a process contributing essentially to both upper and lower active levels of Ne-like ions at lower electron temperatures (around 30-40 eV).

Kinetics calculation for Ni-like ions turned out to be much more complicated than for Ne-like Ar mainly due to a limited computer power. We did not plan to perform calculations for Ni-like ions in Phase I. Howerver, we did get the work started. We expect to complete these calculations in Phase II, as Ni-like Ar is very attractive lasder medium, requiring lower temperatures to populate

upper laser levels yet having shorter wavelength transitions.

For the calculated populations in Ne-like Ar we also estima. d a small signal gain and possible amplification for different lines in the proposed geometry (2x100 mm) of a capillary discharge x-ray laser driver (see Table 2.)

Table 2. Estimated gain (in cm^{-1}) for different transitions in Ne-like Ar in the 2x100 mm capillary discharge plasma, and related amplification of spontaneous emission.

	T_e (eV)			30	60	30	60
	N_e (10^{18} cm^{-3})			1	1	10	10
#	Transition	Wavelength (nm)	Gain G (cm^{-1}), GL product and related amplification I/I_0 = exp(GL)				
1	12-4	69.76	G	.57E-3	.58E-1	.79E-2	.12E+1
			GL	.57E-2	.58E 0	.79E-1	.12E+2
			exp(GL)	1.006	1.786	1.082	1.6E5
2	11-4	71.25	G	.12E-3	.68E-2	.21E-2	.25E 0
			GL	.12E-2	.68E-1	.21E-1	.25E+1
			exp(GL)	1.001	1.070	1.021	12.18
3	10-4	72.75	G	.15E-3	.19E-1	.25E-2	.39E 0
			GL	.15E-2	.19E 0	.25E-1	.39E+1
			exp(GL)	1.002	1.209	1.025	49.4
4	14-2	43.07	G	.51E-3	.40E-1	.28E-2	.48E 0
			GL	.51E-2	.40E 0	.28E-1	.48E+1
			exp(GL)	1.005	1.492	1.028	121.5
5	28-2	15.8	G	-.35E-6	.41E-3	.17E-4	.13E-1
			GL	-.35E-5	.41E-2	.17E-3	.13E 0
			exp(GL)	.99999	1.004	1.002	1.14

Calculations of gain for other temperatures and densities were also performed (not shown in the Table 2). It was found that a gain for the strongest transitions 12-4 and 10-4 reachs a maximum at electron temperatures around 50-60 eV and densities 10^{19} cm^{-3}. At higher densities gain decreases essentially as a consequence of collisional mixing of upper and lower active levels as well as due

to a reabsorption of a radiation from the lower active levels in a capillary plasma. The last effect plays major role in controlling gain in our capillary discharge plasma at high densities, as plasma becomes optically thick in Ne-like Ar resonance lines.

As can be seen from Table 2, the GL product for the proposed x-ray laser driver could be high enough for 10-cm plasma column. For the strongest transition 12-4 GL reachs the value 12, which is usually considered close to a saturation regime. The next strongest transition is the short-wavelength 14-2 transition, which shows possible a GL value 4.8 and amplification more than 10^2. The two transitions 10-4 and 11-4 show moderate GL=3.9 and 2.5, respectively. This results in moderate amplification of 50 and 12, which, nevertheless is still possible to observe experimentally. At last, the shortest-wavelength transition, 28-2 (15.8 nm) has a negligible amplification.

For the Ar plasma with an ion temperature of 50-60 eV the Doppler width lies in a range $\Delta\lambda/\lambda \simeq 10^{-4}$. A low- and medium-resolution spectrometer will measure intensity integrated over an instrumental profile. To measure the gain properly, an integral equation for a given instrumental factor and line shape should be solved. Fortunately, it was found [5] that for any sharply peaked line profile, including Doppler, the following analytical dependance of measured intensity on the gain serves as a good approximation of the exact solution for this equation:

$$I = J\frac{(\exp(GL)-1)^{3/2}}{G^{3/2}(L\exp(GL))^{1/2}}$$

Here I = measured line intensity, G = gain, L = length of amplifying media, J = intensity of plasma spontaneous emission per unit length. This dependance was found to be the most correct and widely used for an experimental gain measurement. We will use this equation to derive a gain in our experiment.

3. CAPILLARY DISCHARGE PLASMA MHD SIMULATION

To determine the plasma temperature, density, velocity and ion abundances, a magnetohydrodynamic (MHD) code (simulating capillary discharge plasma) was created. Actually we started with an implementation of the "PINCH" MHD code developed at Los-Alamos National Laboratory for high-curren deuterium Z-pinch plasma

modelling. We quickly discovered that the code does not describe a capillary discharge plasma at all. We tried to simulate the available capillary discharge experiments but we could not get agreement between temperature and density measured in these experiments and values predicted by "PINCH". This was mainly due to the fact that the capillary wall processes were not accounted for in the code. Modifications of the code did not help much, so we wrote our own MHD code for a capillary discharge plasma geometry.

The one-dimensional (capillary discharge plasma radius dependent) MHD code was created. The code includes a standard set of plasma MHD equations [7] to mass, momentum and energy conservation (where energy is the sum of thermal, kinetic and magnetic energy), and Faraday's and Ohm's law equations. These equations are coupled with radiation energy loss and electron thermal conductivity loss equations.

A Crank-Nicholson-like scheme was developed and adapted to the problem and used to solve the above set of time and space dependent differential equations.

Plasma with parameters typical for a capillary discharge was found to be optically thick for resonance UV and for soft x-ray radiation at a length over 100 μm; thus, to begin with, a blackbody approximation was assumed for radiation loss in $1<h\nu<100$ eV. A real plasma radiation loss differs from a blackbody one (especially for lower densities). To correctly account for it and to approach more closely to a real experiment, the factor for radiation loss was introduced and is an adjustable parameter in the MHD calculations.

The code was tested to simulate Bogen's experiment [6]. The polyethylene capillary they used was 2 mm in diameter and 20 mm in length. The circuit capacitor was 0.3 μF charged with 40 kV maximum and the circuit inductance was 200 nH (see Table 1 of Report #1 for more details). The average ion density was estimated as 10^{18} cm^{-3}.

The result of the temperature simulation is shown by the solid curve in Fig. 3. The dashed curve represents Bogen's measurements of temperature versus time. Since the experiment began from a vacuum capillary in which the initial plasma density is zero, we do not expect our model to simulate early development of Bogen's discharge. What we intend to do here is to simulate the cooling part. Figure 3 shows that our rise time is longer than in the experiment. However, the result shows that the plasma does cool down from $\simeq$ 42 eV to $\simeq$ 16 eV in about the same amount of time. Thus the experiment and the simulation have about the same cooling rate.

Figure 4 illustrates the power contribution of the different processes. The solid curve is **E** x **B** heating power, while the dash curve and the dot dash curve represent the thermal cooling power and radiation power, respectively. From the figure, we see that the

electron heat conduction to the walls of the capillary is about triple the radiation cooling. Milchberg et al [7] built a simple model in which they compared the rate of thermal cooling, radiation cooling and expansion cooling in a carbon capillary device and found that the thermal cooling is significantly larger than the other two. Thus the thermal conduction cooling mechanism which plays a major role here is consistent with Milchberg's result.

The two total current comparisons show a difference of less than a few percent. This is an excellent match and it shows us that the magnetic field boundary condition is correct at relatively low temperatures (here less than 50 eV). This also gives us a strong clue that the code does behave properly since the magnetic field at the wall is determined not only by the external electric field but also by pressure, density, thermal force, and the degree of ionization.

The ion abundance evolution calculated using the general Saha equation is illustrated in Fig. 5. In this figure, 1 denotes neutral carbon, 2 = B-like ion, 3 = Be-like, 4 = Li-like carbon, and 5 = He-like carbon. At the cooling time (from 0.3 to 0.5 μs) He-like ions dominate the abundance which is consistent with the experiment. Figure 6 shows the plasma resistance evolution curve. The average value is about 1 ohm. The ohmic heating power I^2R for current I = 30 kA is about 1 GWatt, which is enough to heat up the plasma to 45-50 eV during a 150-200 nsec time interval.

The major advantage of our model is that we can monitor the 1-D space distribution for several quantities. Figure 7 to 11 show the density, velocity, magnetic field, pressure and temperature distribution as a function of radius and time. Since the electric field E points in the z direction and the magnetic field B is in the θ direction, the resulting force $E \times B$ will shift the plasma into the center (pinch-effect). This can be seen in fig. 7. Figure 8 shows that the velocity begins from 0 and goes negative first, which is consistent with a z-pinch. The fluid then sloshes back and forth, as expected for MHD waves. Because of magnetic confinement, and because of the thermal conduction and radiation cooling to the wall, the pressure is higher in the center and lower at the edge as shown in Fig. 10. The temperature behaves the same way but with a different slope due to density gradient, as shown in Fig. 11.

The 1-D MHD code has successfully passed several analytical tests and was found to correctly interpret experimental data.

This code has been used to simulate our future experiment with Ne-like Ar. The result of this simulation is shown in Figs. 12-19 for 2x100 mm capillary filled with Ar at the initial pressure 5 mm Hg. Fig. 12 shows a radiated loss in an Ar plasma during discharge. Plasma resistivity versus time is shown in Fig.13. The circuit impedance VL/C for effective plasma heating should be choosen

close to plasma resistivity, i.e. should be in 2-5 ohm range. Ion fluid velocity distribution across the capillary radius is shown in Fig. 14. The magnetic field in our capillary discharge is shown in Fig. 15. Pressure of plasma (which is mainly electron component pressure) is shown in fig. 16. Note essintually lower pressure near the capillary wall compared to pressure near the center due to magnetic confinement - this helps to reduce shock load to the capillary wall during discharge. Fig. 17 shows Ar ion density distribution across the capillary. Ion abundances history versus discharge time is shown in Fig. 18. Here 0 represent neutral gas, 8+ - Ne-like Ar. More than half of total Ar ions are ionized to Ne-like stage. Temperature distribution in Ar capillary discharge is showm in Fig. 19. Temperature approaches 60 eV near the capillary center.

Currently the code is under development for simulations of a Ni-like Kr plasma capillary discharge.

As shown above, a macroscopic gain in a capillary discharge plasma may be achieved for a Ne-like Ar plasma with electron temperatures of 50-60 eV and electron density of around 10^{19} cm^{-3}. The calculated gain is high for the strongest 12-4 transition (69.76 nm) and more modest for the three others. It could be lower in a real plasma especially for plasma with non-optimal parameters. Hence, a long length (10 cm) capillary should be used. According to the MHD simulation, plasma with the necessary initial density of a neutral Ar may be heated up to a 50-60 eV temperature and confined in the 1-mm radius capillary during several hundred nanoseconds (time required to get enough abundance of Ne-like Ar at this electron density). The required discharge current is a reasonably modest 20-30 kiloamps. To drive such a current during hundreds nanoseconds through 1x100 mm plasma, a capacitor of 0.1-0.2 μF should be used and it should be charged to 40-50 kV. To allow rapid current rise, the inductance of the discharge circuit should not exceed 0.2-0.5 μH.

IV. CAPILLARY DISCHARGE X-RAY LASER DESIGN.

Using the results of above described simulation of Ar capillary discharge, we designed the experimental device.

We have began building the capillary discharge x-ray laser driver with the following discharge circuit parameters: C = 0.22 μF, L = 0.1-0.2 nH, U = 30-70 kV, maximum energy stored in the capacitor E = 500 J.

The capillary geometry could be varied, and for the first

experiment a 2 x 100 mm capillary was chosen. The length was chosen longer than for ordinary capillaries to achieve better amplification for lines with a lower gain coefficient in real plasma. The gas-filled spark gap switch provides the discharge triggering. This switch is attached to one end of the capillary, while another one is open for diagnostics. Two extra side ports in the capillary discharge holder provide access to the quarts capillary and can be used for observation of the plasma in visible and near UV light. The device is very compact: 6x2x3 dm^3 without the capacitor and vacuum pump, and even not much larger with both. It is really table-top x-ray laser driver.

The design of the capillary discharge is shown in Fig. 20.

CONCLUSIONS.

Atomic and kinetics calculations along with MHD simulation have shown that the proposed capillary discharge plasma will serve as an active media for soft x-ray laser driver. Calculations for Ne-like Ar have shown that a medium-energy capillary discharge plasma should have parameters favourable for obtaining ASE in Ne-like Ar, with a gain in the range 0.3-1 cm^{-1} for long-wavelength 3p-3s transitions ($\simeq$70 nm) and 0.4 cm^{-1} for shorter wavelength ($\simeq$43 nm). To explore such a gain, a 10 cm length capillary with 0.5 kJ stored energy is under construction now. Several 4d-4p transitions in Ni-like Kr (with $\lambda \simeq 30$ and 40 nm) have also been found to be the potential lasing lines for Kr filled capillary with lower temperature plasma. Kinetics calculation for a gain estimation in Ni-like Kr plasma and MHD simulation of a capillary discharge optimized for laser transitions in such the plasma are on the way.

The capillary discharge x-ray laser driver is under construction.

Two papers resulted from Phase I research efforts [8,9], and more expected to be published during Phase II to inform scientific community about progress of our capillary discharge x-ray laser project.

REFERENCES:

1.Kanayskas U.M., Rudzikas Z.B., Sov. Lit. Fis. Sb., 1, 13, 191 (1975)

2.Driker M. M., Ivanov L.N., Sov. J. Opt. Spectroscopy, 49, 209,

(1980)

3. D. G. Hummer and G. B. Rybicki, *Astrophys. J.*, **254**, 767 (1982).

4. R. A. London, "Line escape probabilities for exploding foils", in Laser Program Annual Report 86, M. R. Rufer and P. W. Murphu, eds., Univ. of California Report No UCRL 50021-86 (LLNL, California, 1988)

5. G. J. Linford, E. R. Peressini, W. R. Sooy and M. L. Spaeth, Appl. Optics 13, 379 (1974)

6. P. Bogen, H. Conrads, D. Rusbueldt, Z. Physik 186, 240 (1965).

7. H. Milchberg, C. H. Skinner, S. Suckever, and D. Voorhees, *Appl. Phys. Lett.*, **47**, 1151 (1985).

8. L. V. Knight, A. M. Panin, B. G. Peterson and E. P. Ivanova, "Possibility of observing x-ray laser lines using a capillary discharge plasma", XV International Conference on LASERS '92, Huston, Texas.

9. L.V.Knight, A.M.Panin, B.G.Peterson, E.P.Ivanova, "Possible soft x-ray laser lines in a capillary discharge plasma", Physica Scripta (in press).

FIGURE CAPTIONS.

Fig. 1. Calculated population of levels of Ne-like Ar in the capillary discharge plasma for T_e=60 eV, N_e=10^{18} cm^{-3}.

Fig. 2. Calculated population of levels of Ne-like Ar in the capillary discharge plasma for T_e=60 eV, N_e=10^{19} cm^{-3}.

Fig. 3. Temperature comparison between our simulation and Bohen's experimental result.

Fig. 4. Power contribution of different physical processes in simulation of Bogen's run.

Fig. 5. Ion abundance in simulation of Bogen's run.

Fig. 6. Plasma resistance in simulation of Bogen's run.

Fig. 7. Ion density in simulation of Bogen's run.

Fig. 8. Plasma velocity in simulation of Bogen's run.

Fig. 9. Magnetic field in simulation of Bogen's run.

Fig. 10. Pressure in simulation of bogen's run.

Fig. 11. Temperature in simulation of Bogen's run.

Fig. 12. Radiated power (W/m^3) for Ar plasma in simulation of capillary discharge x-ray laser driver. Initial Ar atomic density is 10^{17} cm^{-3}, or 4.8 mm Hg, capillary radius is 1 mm, length 100 mm.

Fig. 13. Plasma resistance (Ohm) versus time in the Ar capillary discharge x-ray laser driver.

Fig. 14. Ion velocity (m/sec) in the Ar capillary discharge x-ray laser driver.

Fig. 15. Magnetic field (T) in the Ar capillary discharge plasma.

Fig. 16. Pressure (Pa) in the Ar capillary discharge plasma.

Fig. 17. Ion density (m^{-3}) in the Ar capillary discharge plasma simulation.

Fig. 18. Abundances of different ionization species in the Ar capillary discharge plasma simulation.

Fig. 19. Electron temperature (eV) in the Ar capillary discharge simulation.

Fig. 20. Capillary discharge x-ray laser driver design.

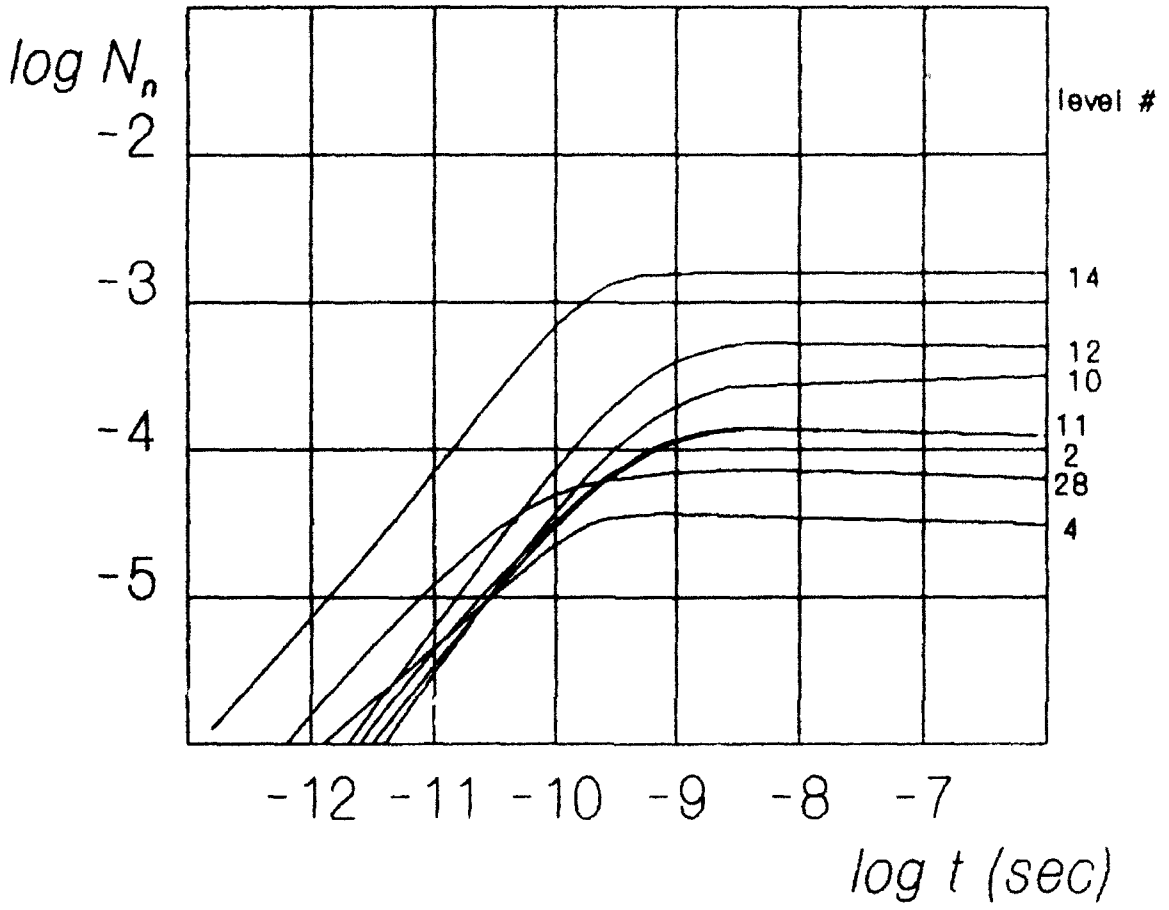

Fig. 1. Level populations versus time for Ne-like Ar in a capillary discharge plasma with T_e = 60 eV, N_e = $10^{18}cm^{-3}$

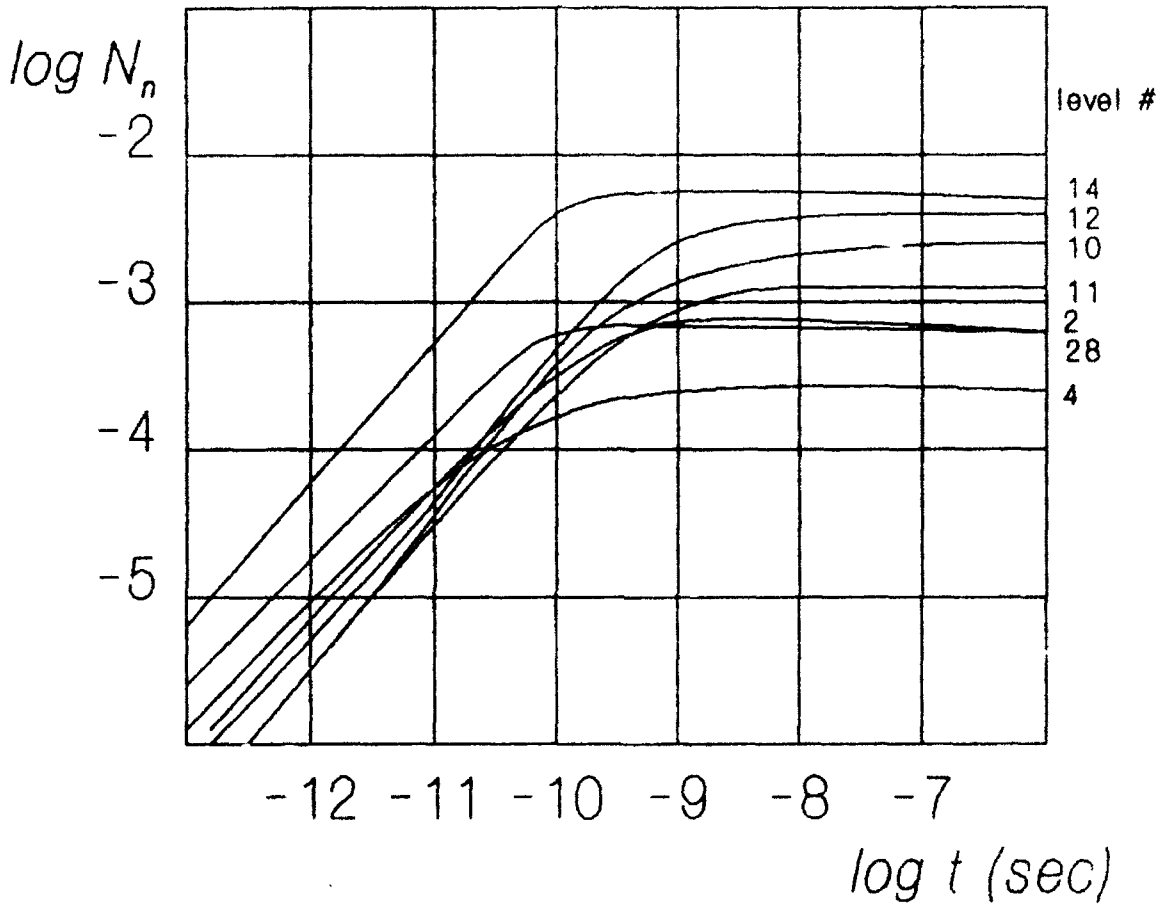

Fig 2. Level populations versus time for Ne-like Ar in a capillary discharge plasma with T_e = 60 eV, N_e = $10^{19}cm^{-3}$

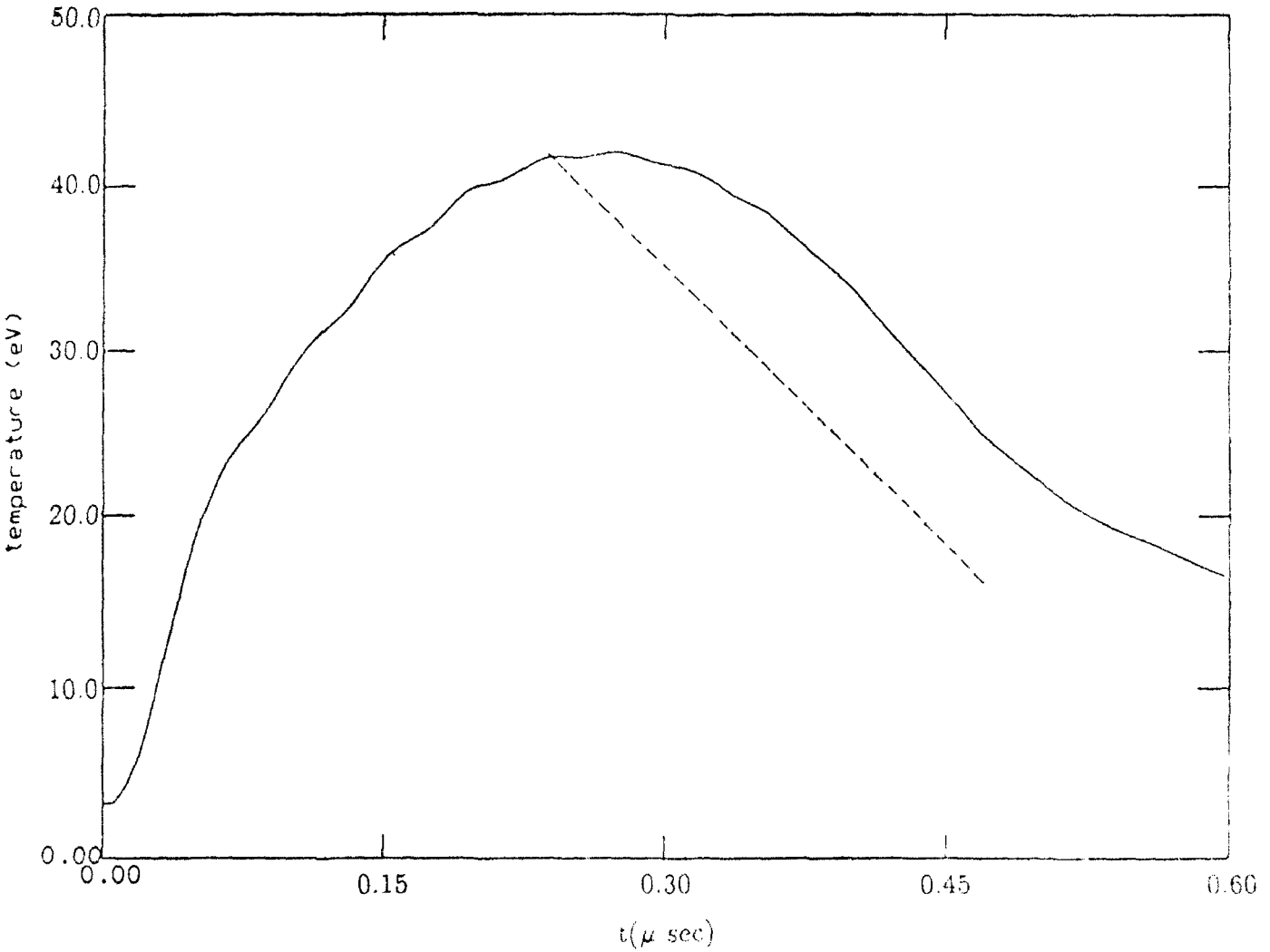

Fig. 3. Temperature comparison between our simulation and Bogen's experimental result (solid line: our simulation, dash line: Bogen's result).

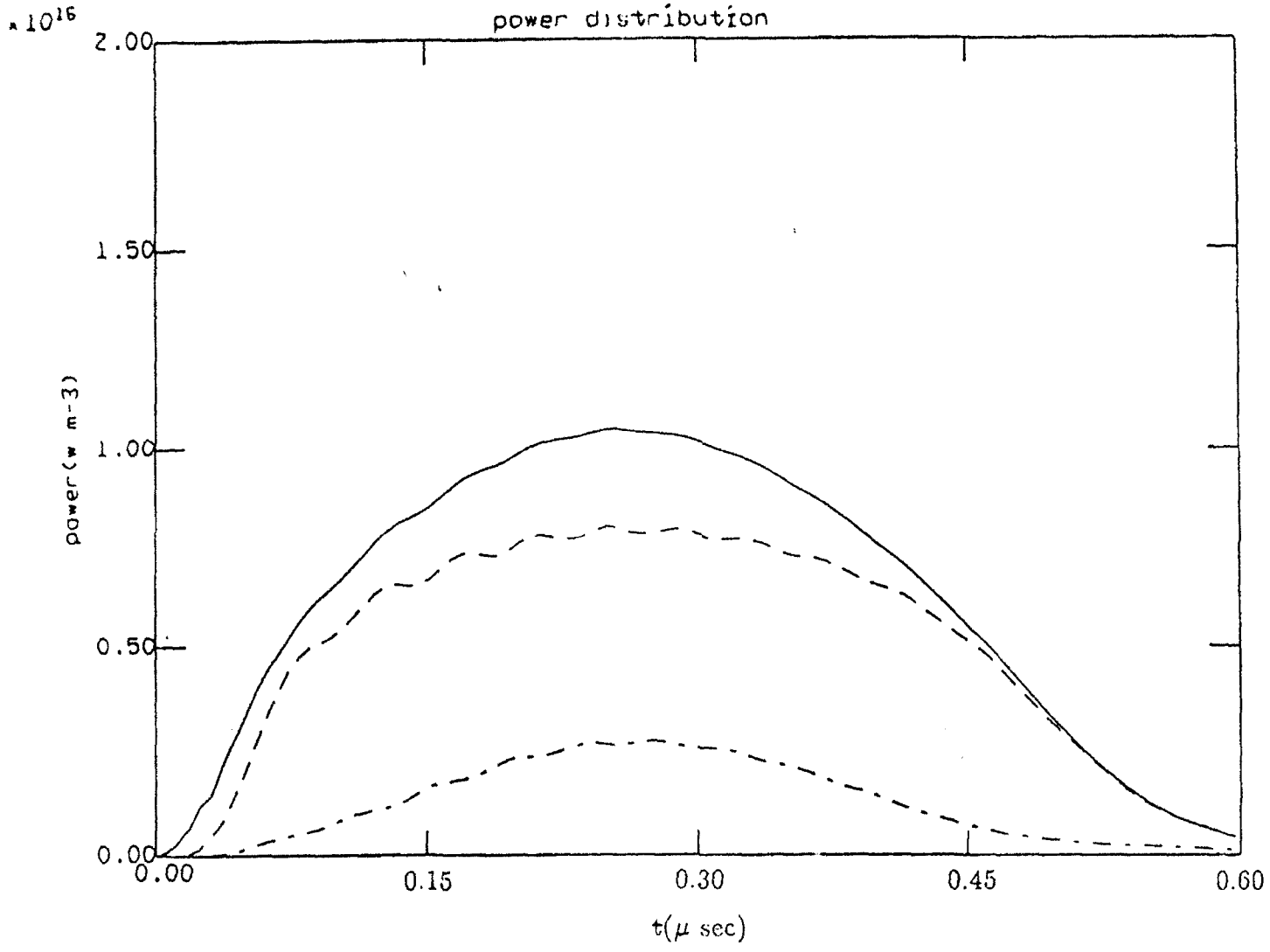

Fig. 4. Power contribution of different physical processes in simulation of Bogen's run (solid line: heating power, dash line: thermal conduction power, dot-dash line: radiation power).

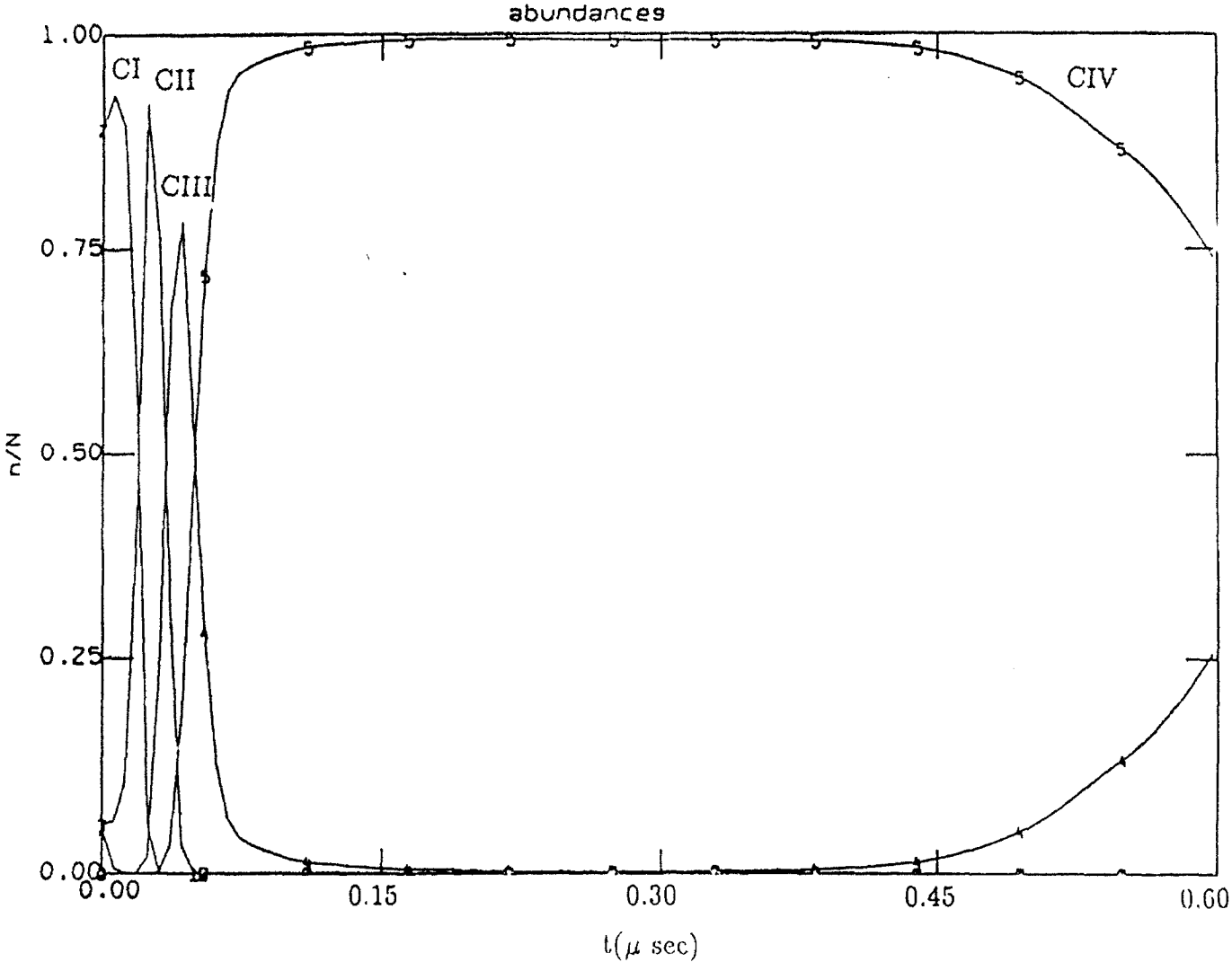

Fig. 5. Carbon ion abundance in simulation of Bogen's run.

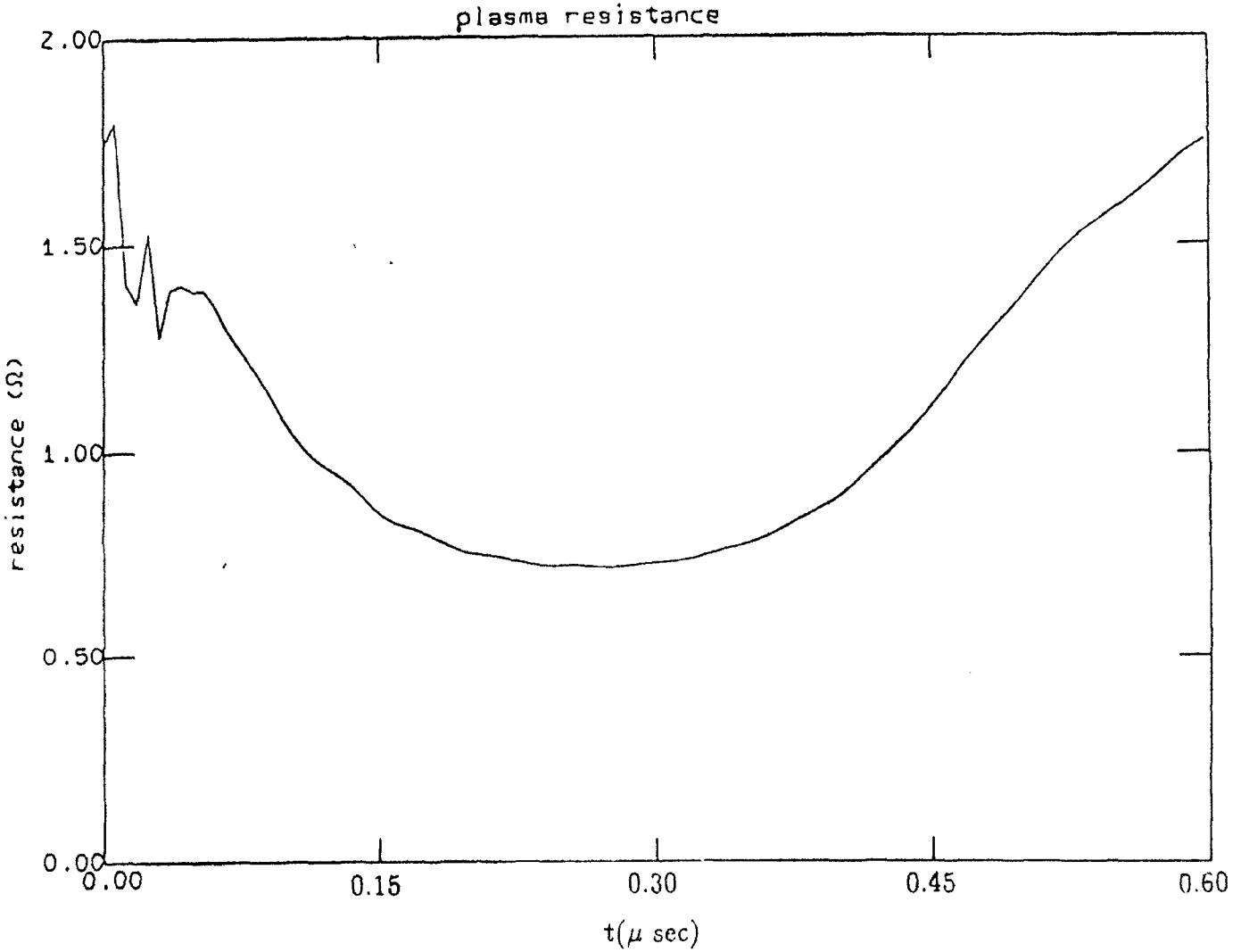

Fig. 6. Plasma resistance evolution curve in simulation of Bogen's run.

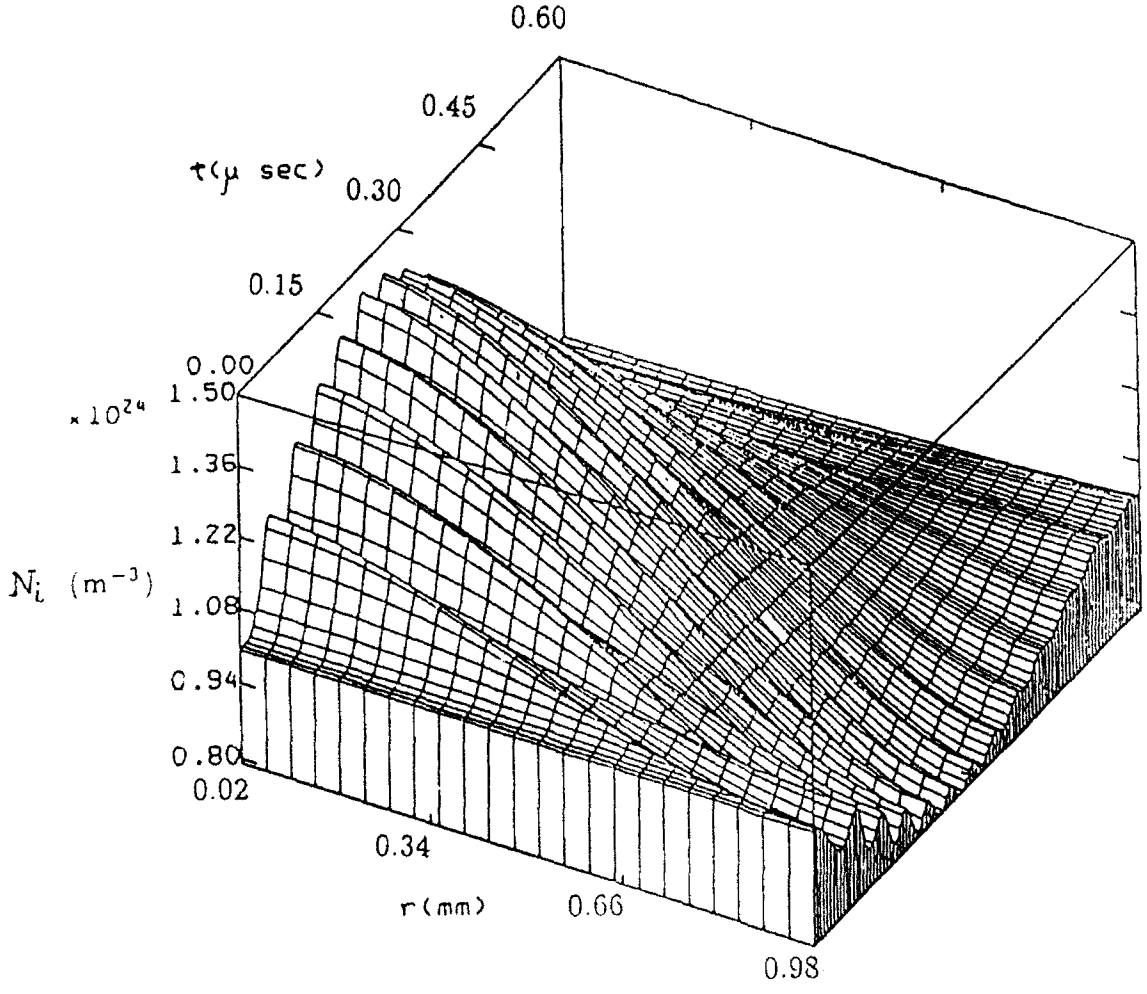

Fig. 7. Ion density in simulation of Bogen's run.

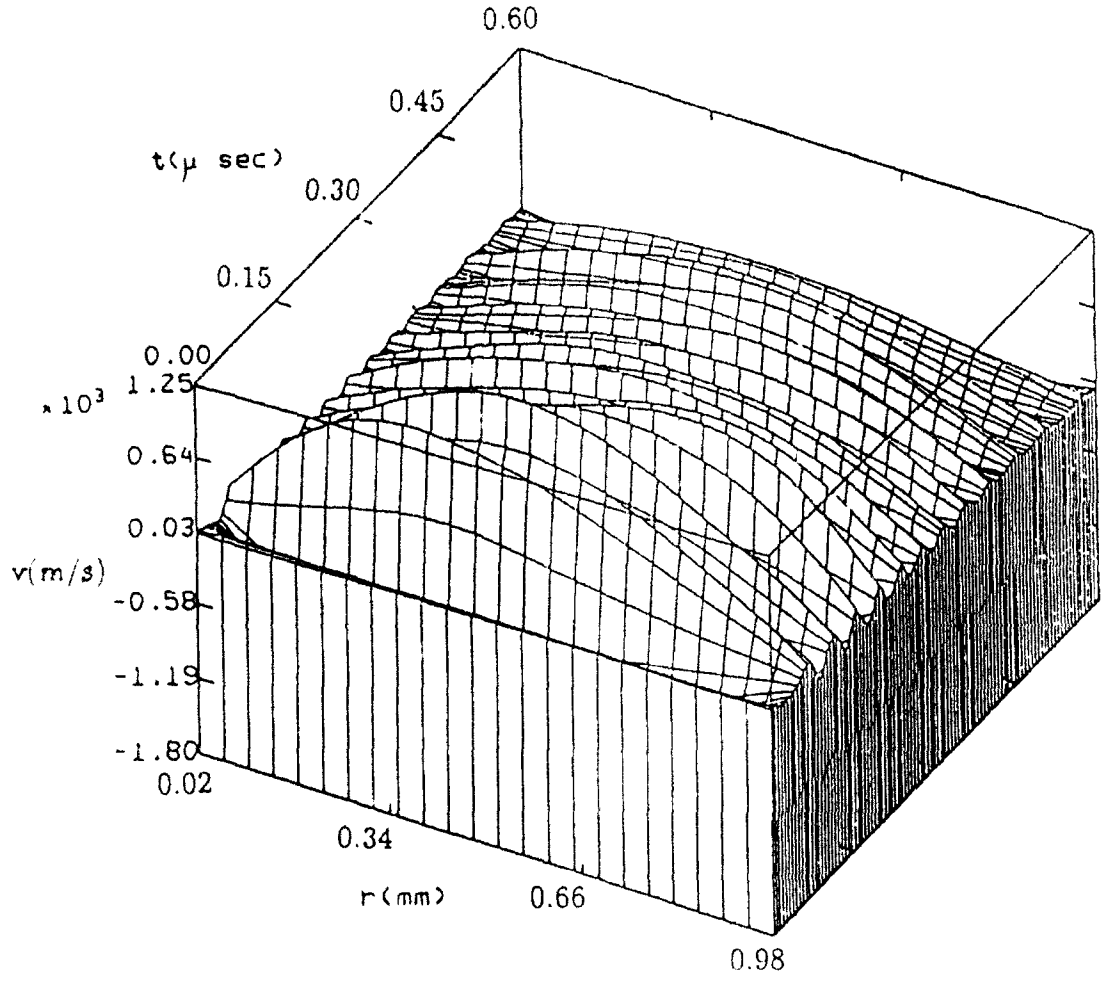

Fig. 8. Fluid velocity in simulation of Bogen's run.

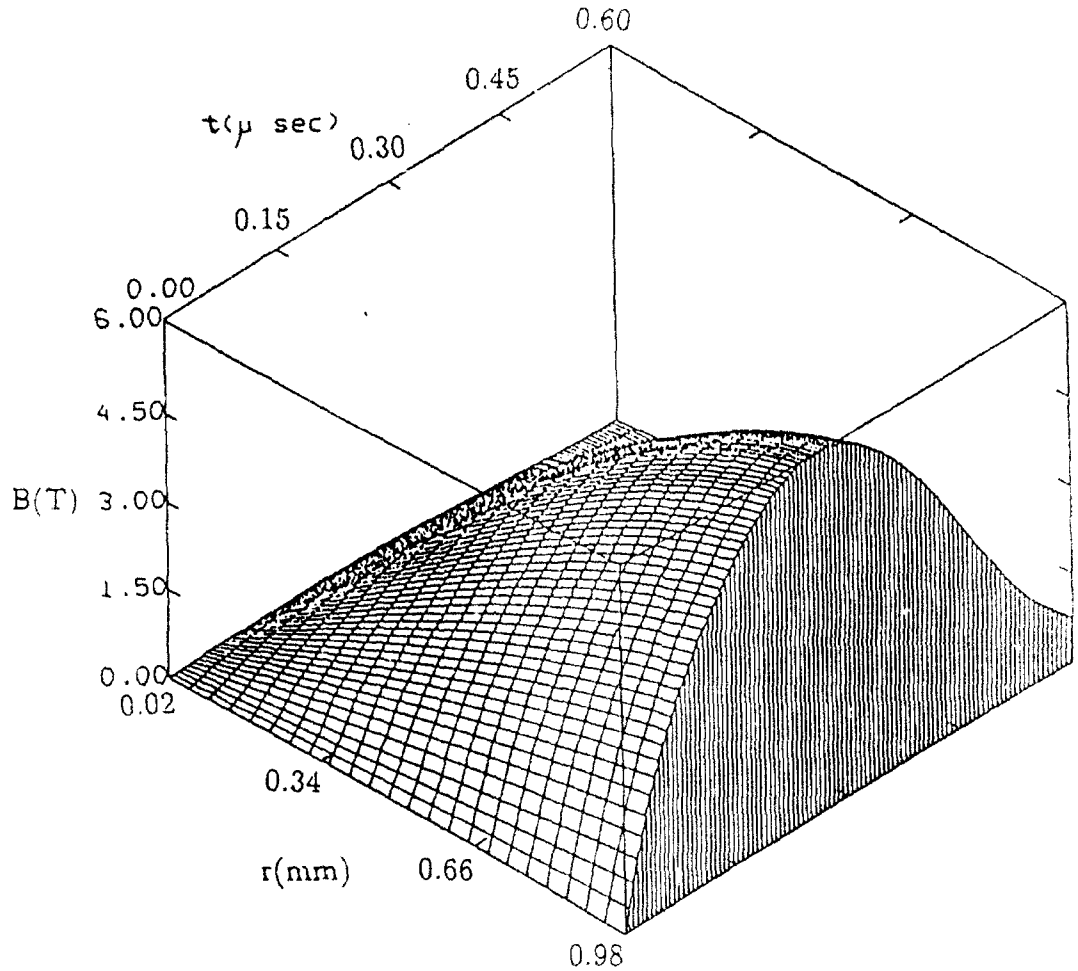

Fig. 9. Magnetic field in simulation of Bogen's run.

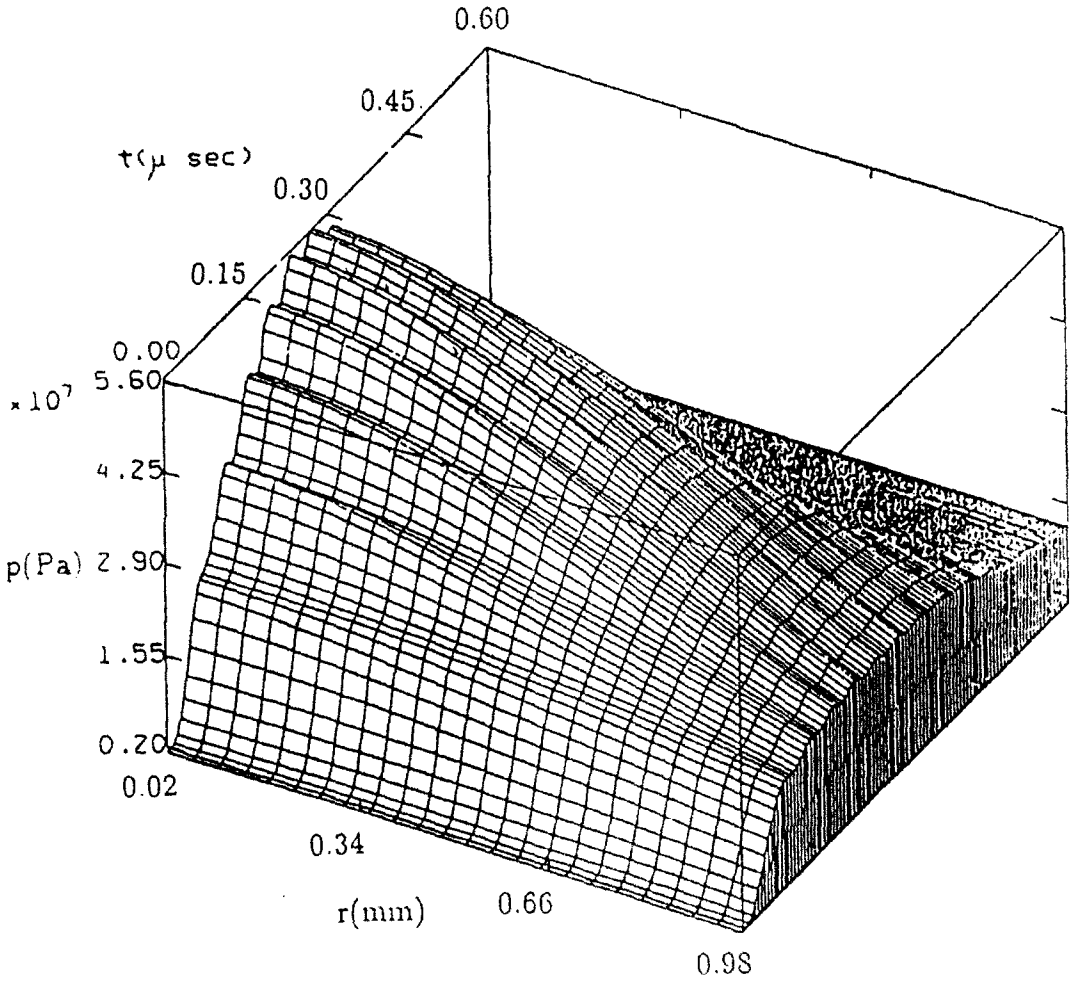

Fig.10 . Pressure in simulation of Bogen's run.

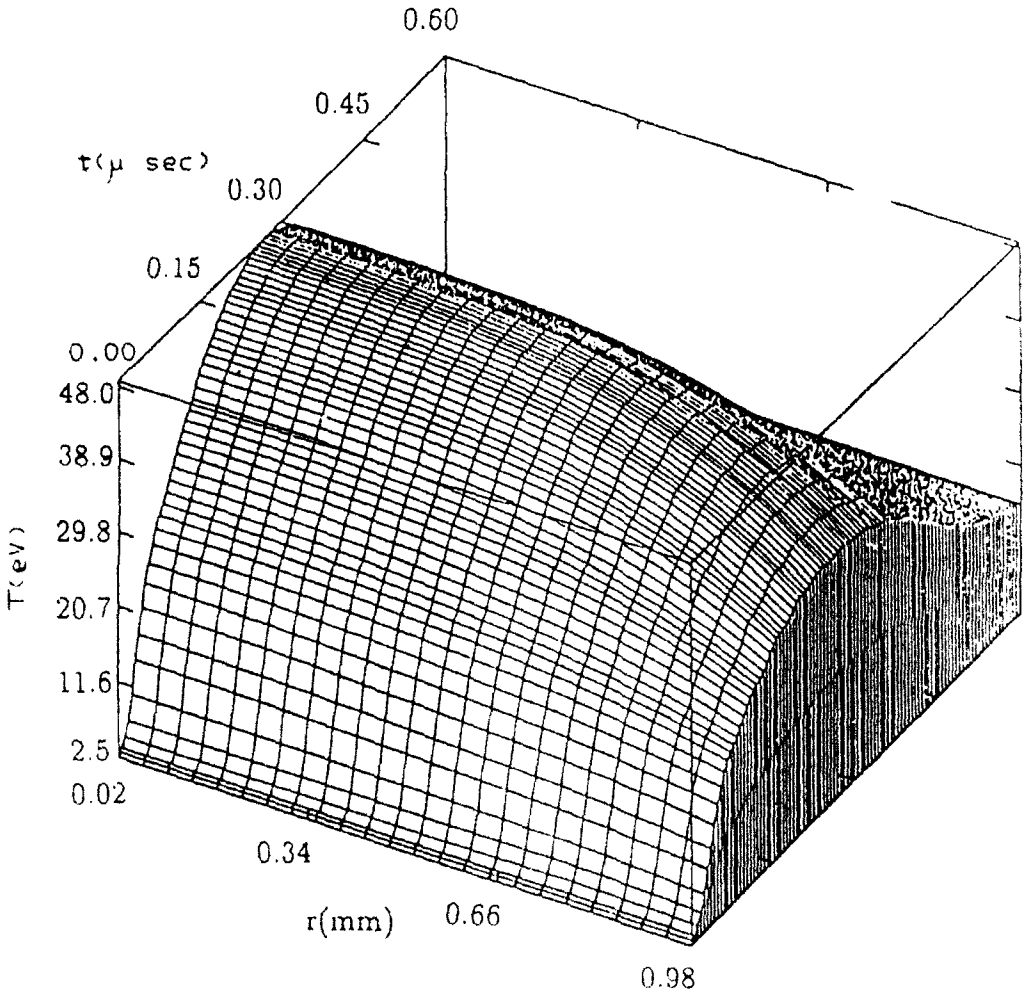

Fig. 11. Temperature in simulation of Bogen's run.

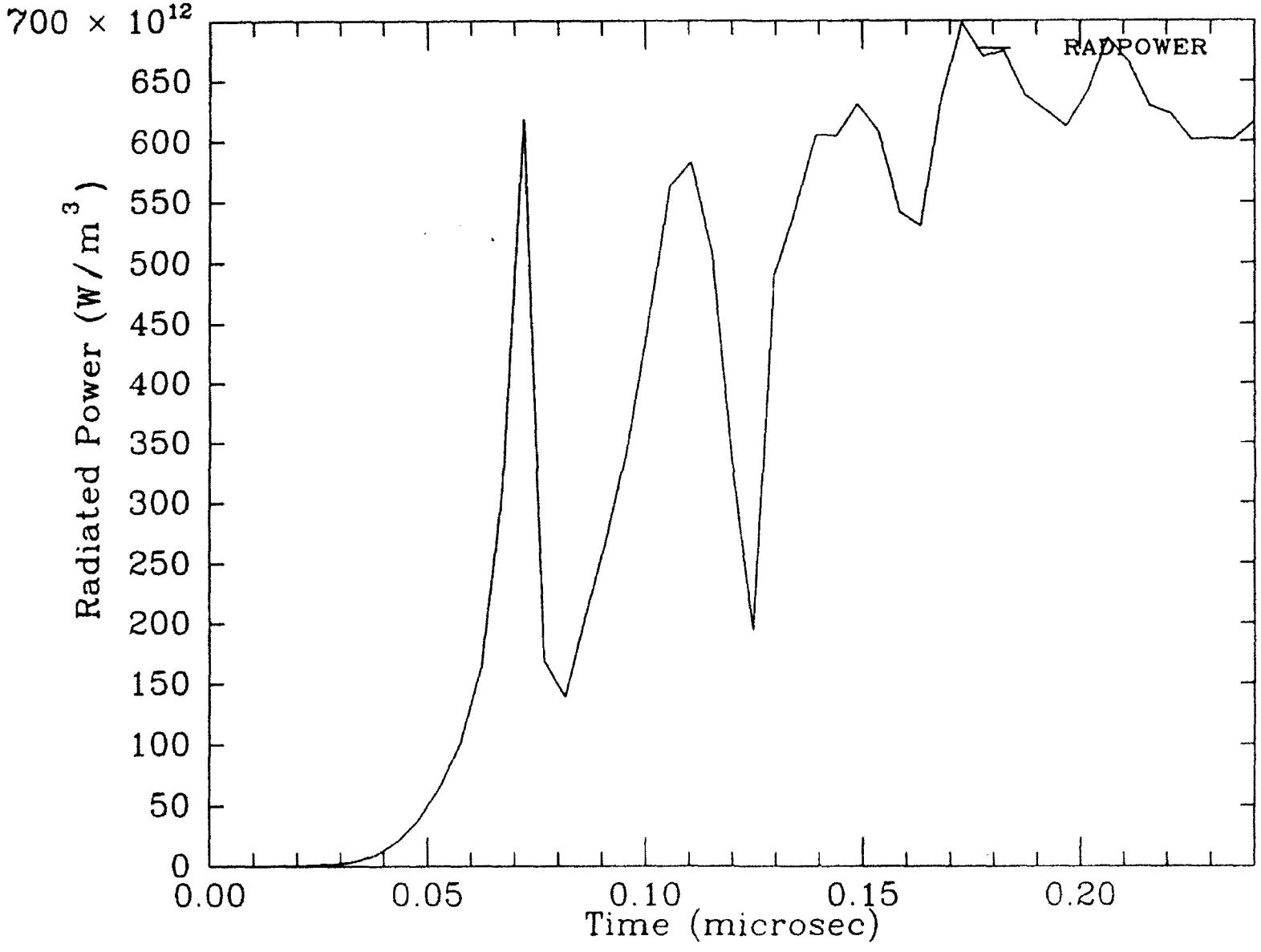
CAPILLARY DISCHARGE MODEL
Radiated Power, 10 cm Ar
700 × 10^12
650
600
550
500
450
400
350
300
250
200
150
100
50
0
Radiated Power (W/m^3)
RADPOWER
0.00
0.05
0.10
0.15
0.20
Time (microsec)
< P L O T 7 9 > Release 2.3 21-MAY-93 17:00:53

Fig. 12.

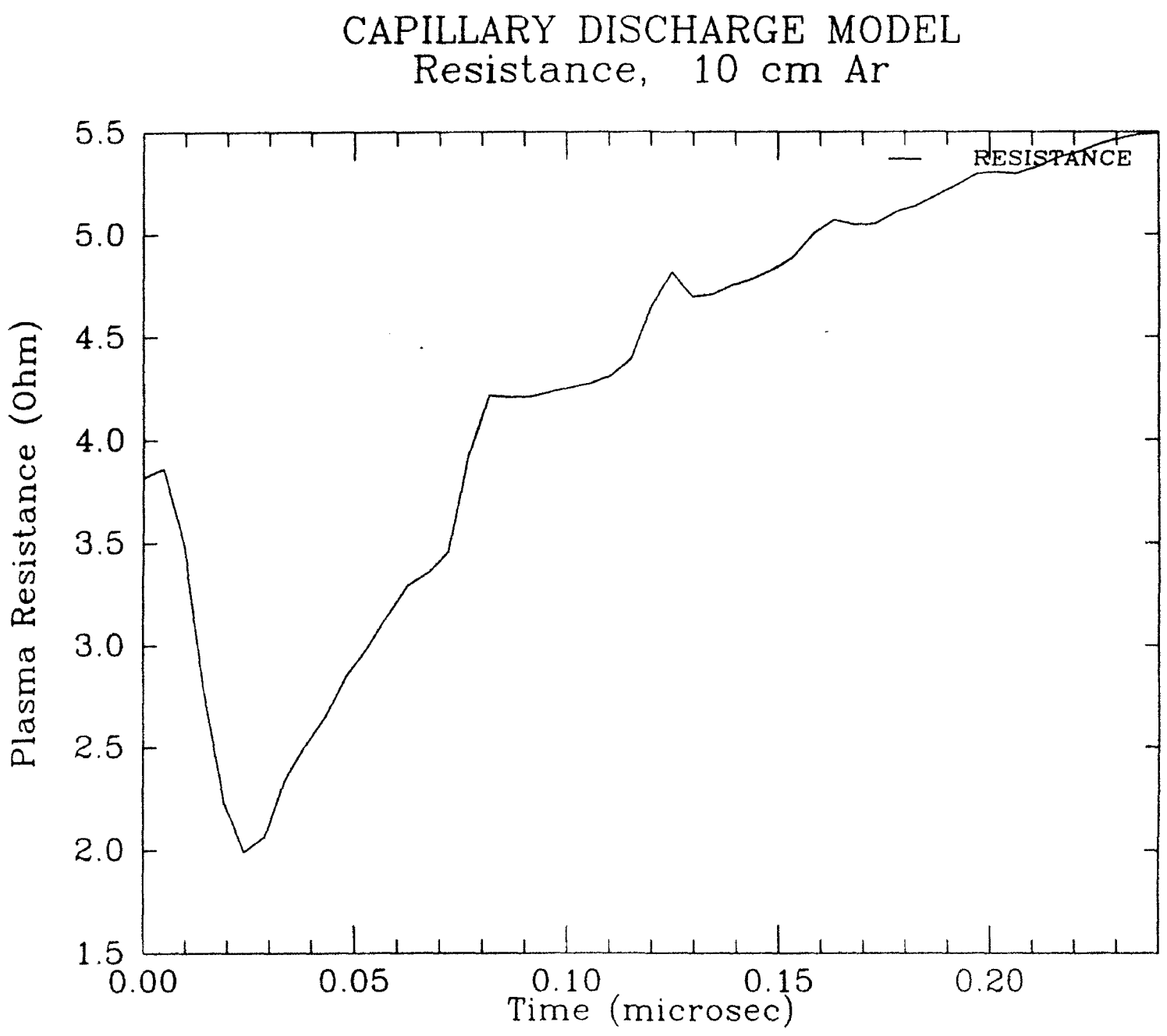
CAPILLARY DISCHARGE MODEL
Resistance, 10 cm Ar
RESISTANCE
Plasma Resistance (Ohm)
5.5
5.0
4.5
4.0
3.5
3.0
2.5
2.0
1.5
0.00
0.05
0.10
0.15
0.20
Time (microsec)
< P L O T 7 9 > Release 2.3 21-MAY-93 17:00:36

Fig. 13 .

Capillary Discharge Model
Ion Velocity, 10 cm Ar

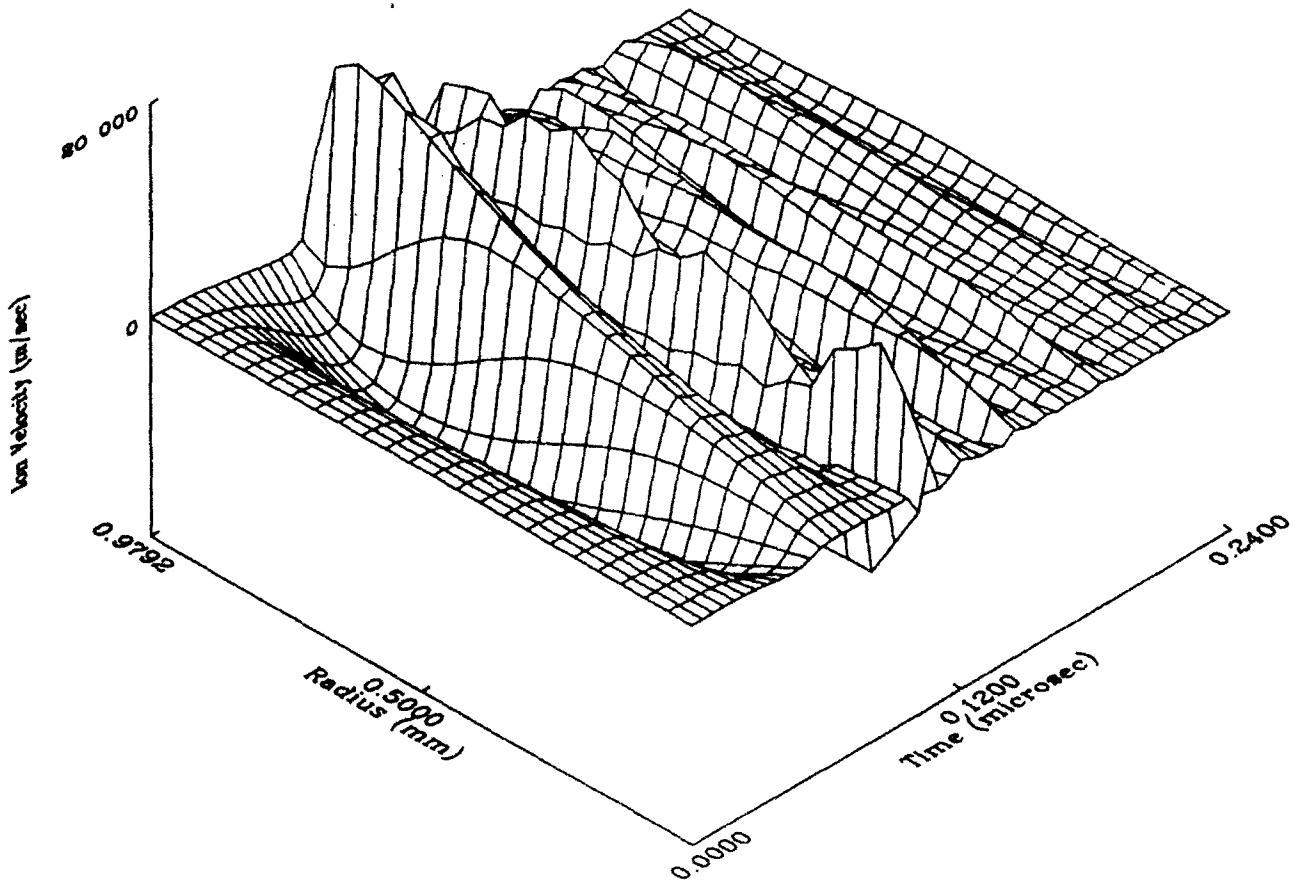

< P L O T 7 9 > Release 2.3 21-MAY-93 16:55:31

Fig.14.

Capillary Discharge Model
Magnetic Field, 10 cm Ar

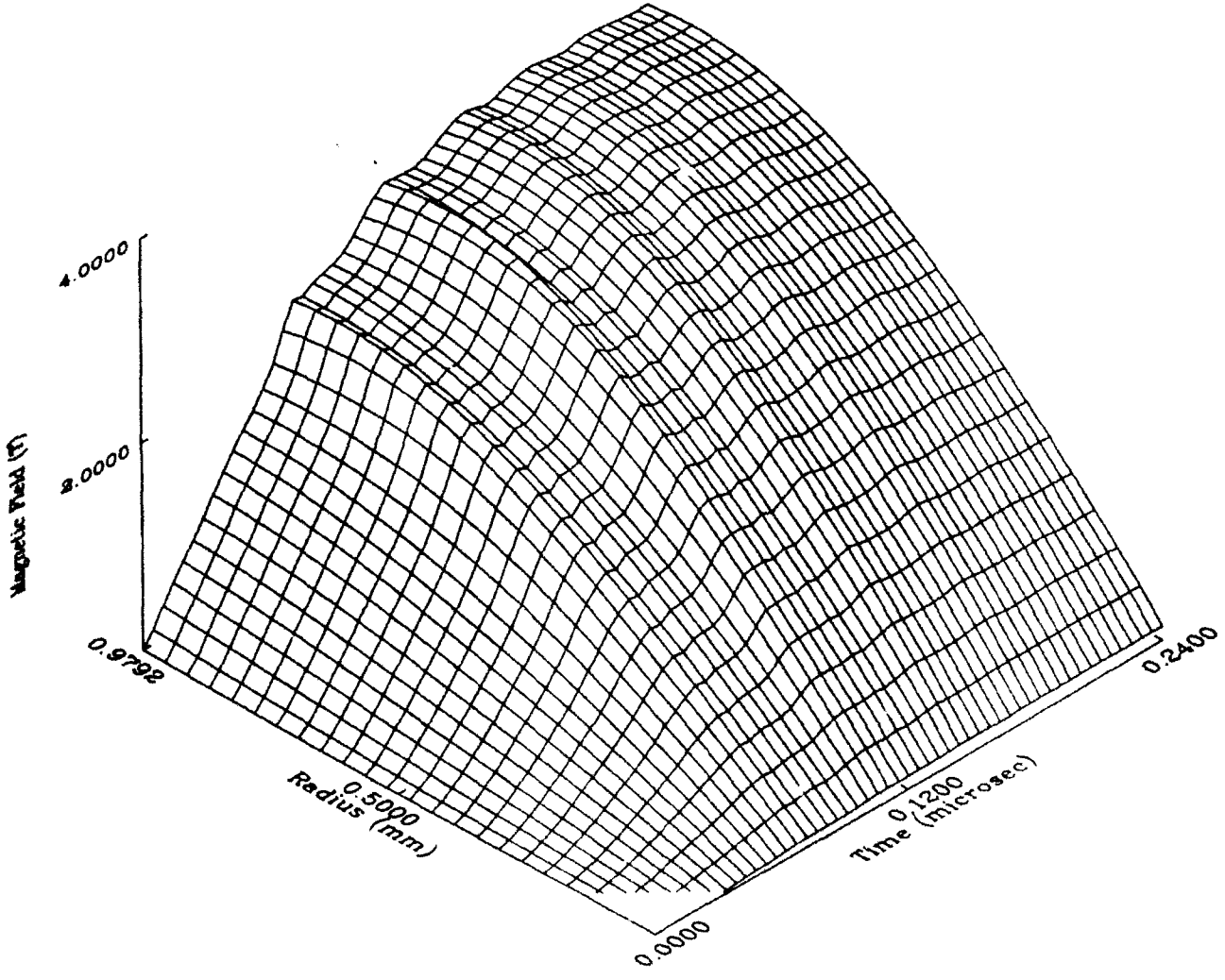

< P L O T 7 9 > Release 2.3 21-MAY-93 16:55:56

Fig. 15.

Capillary Discharge Model
Pressure, 10 cm Ar

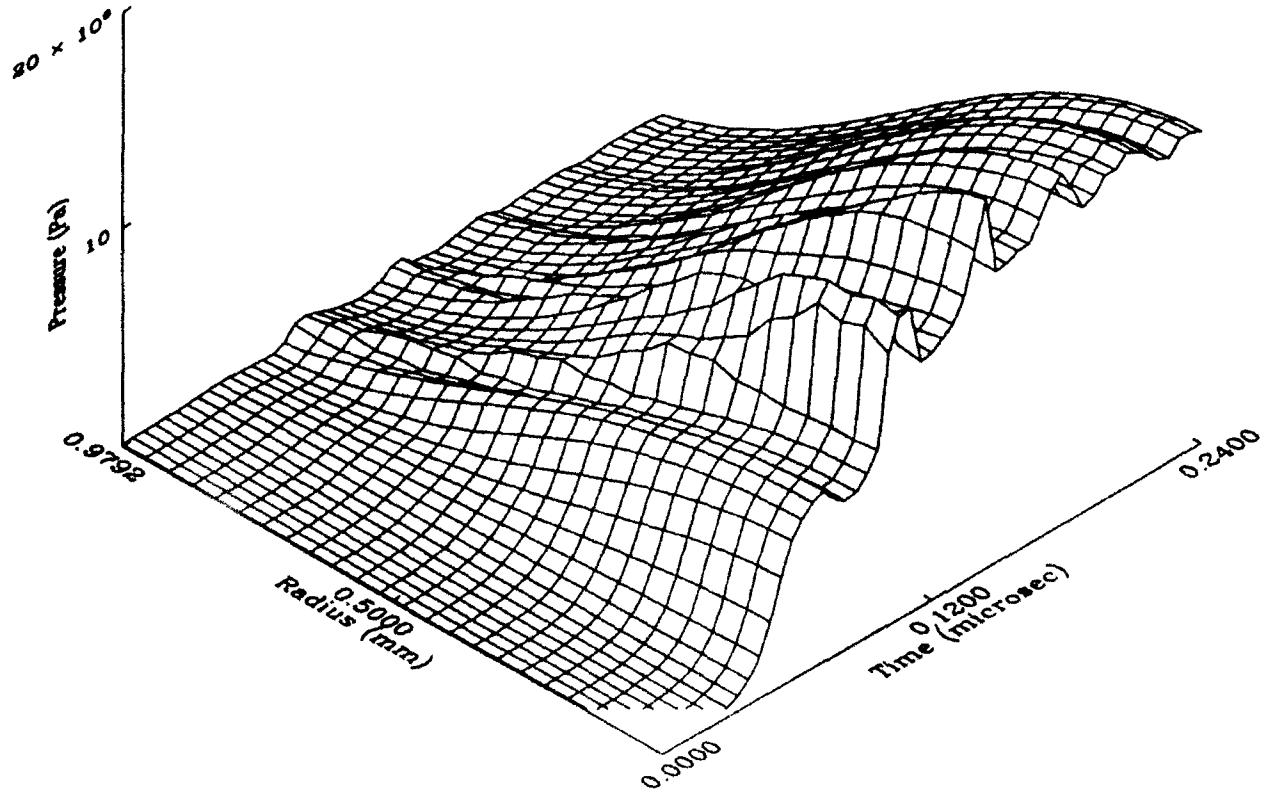

< P L O T 7 9 > Release 2.3 21-MAY-93 16:56:25

Fig. 16.

Capillary Discharge Model
Ion Density, 10 cm Ar

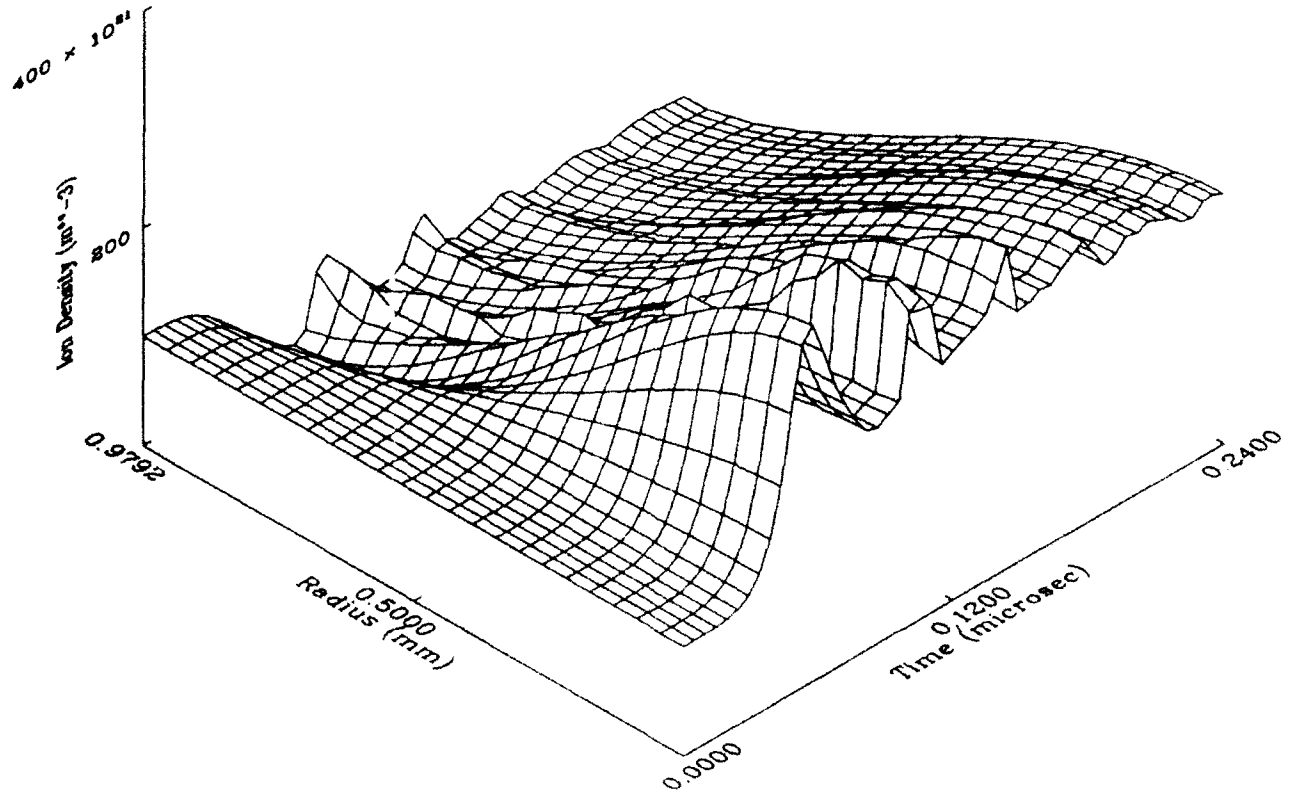

< P L O T 7 9 > Release 2.3 21-MAY-93 16:55:03

Fig. 17.

Capillary Discharge Model
Abundances, 10 cm Ar

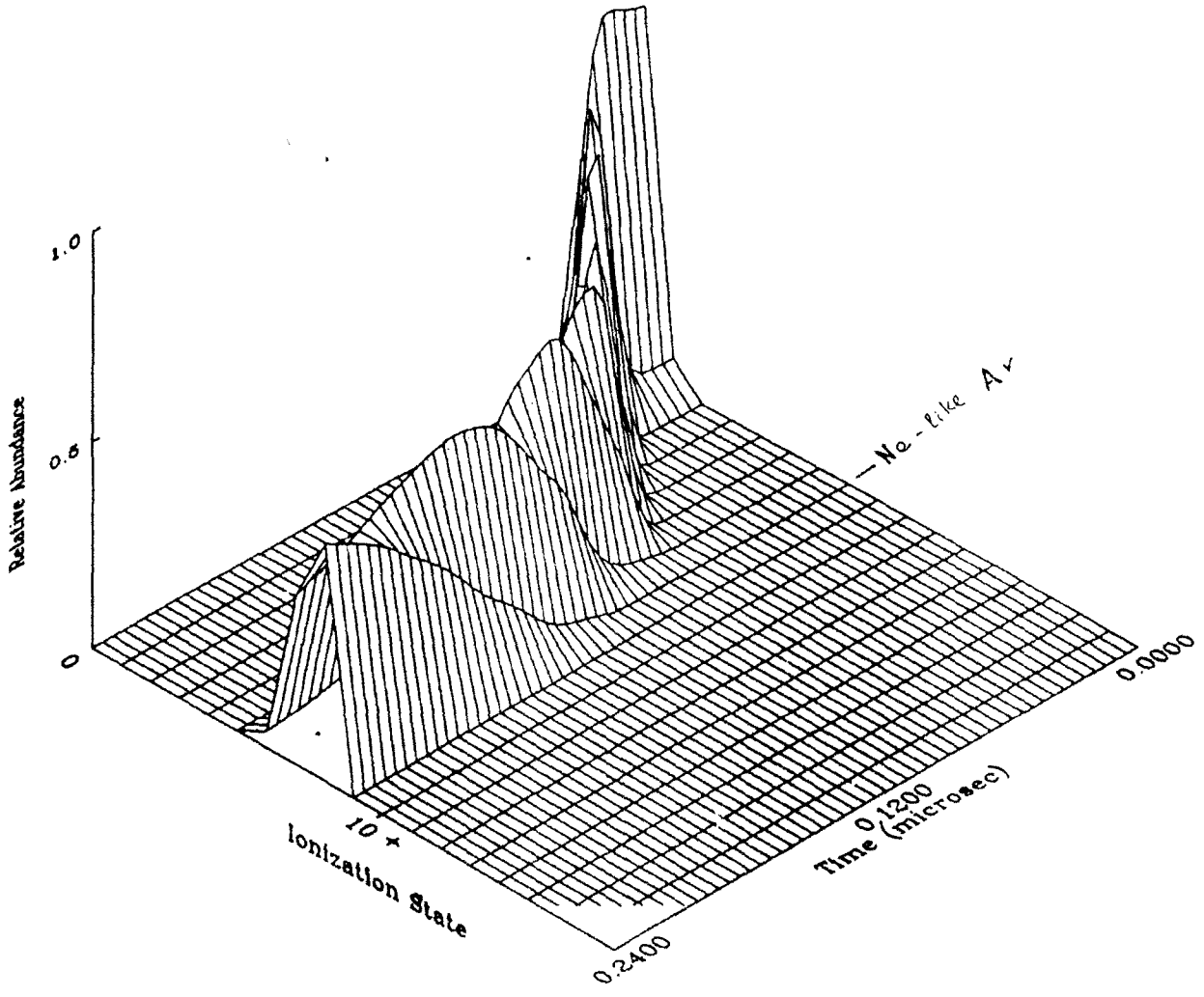

< P L O T 7 9 > Release 2.3 21-MAY-93 16:58:02

Fig. 18.

Capillary Discharge Model
Temperature, 10 cm Ar

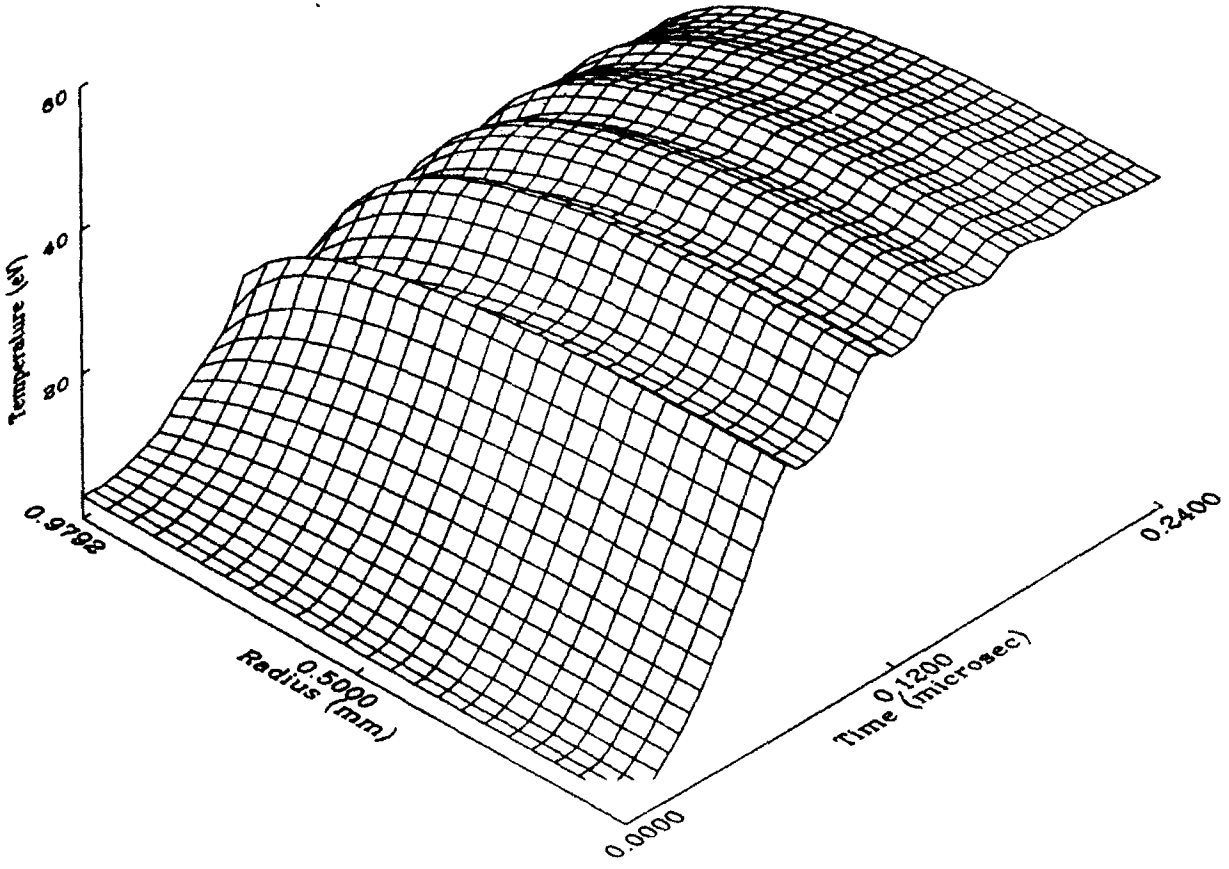

< P L O T 7 9 > Release 2.3 21-MAY-93 16:56:57

Fig. 19.

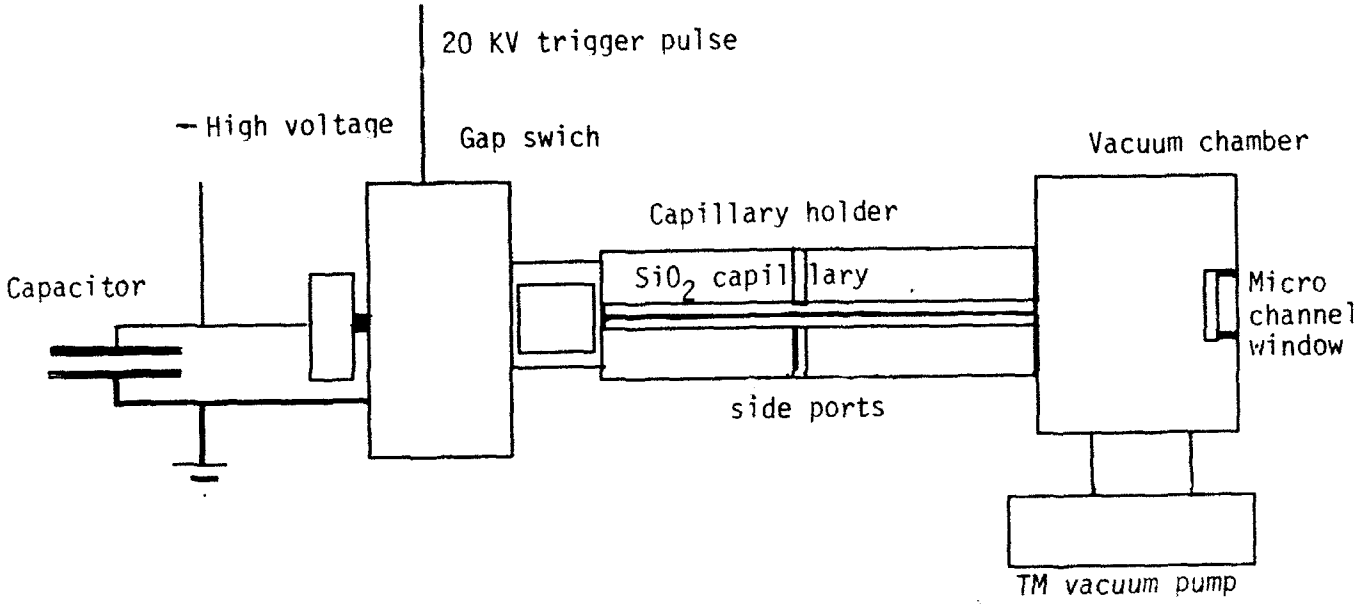

Fig. 20.

Capillary discharge x-ray laser design.